


Boron Clusters | *Hot Paper*

Synthesis, Electronic Properties and Reactivity of $[B_{12}X_{11}(NO_2)]^{2-}$ ($X = F-I$) Dianions

 Knut R. Asmis,^[a] Björn B. Beele,^[b] Carsten Jenne,^{*,[b]} Sebastian Kawa,^[a] Harald Knorke,^[a] Marc C. Nierstenhöfer,^[b] Xue-Bin Wang,^[c] Jonas Warneke,^{*,[a, d]} Ziyang Warneke,^[a] and Qinqin Yuan^[c]

Abstract: Nitro-functionalized undecahalogenated *closo*-dodecaborates $[B_{12}X_{11}(NO_2)]^{2-}$ were synthesized in high purities and characterized by NMR, IR, and Raman spectroscopy, single crystal X-diffraction, mass spectrometry, and gas-phase ion vibrational spectroscopy. The NO_2 substituent leads to an enhanced electronic and electrochemical stability compared to the parent perhalogenated $[B_{12}X_{12}]^{2-}$ ($X = F-I$) dianions evidenced by photoelectron spectroscopy, cyclic voltammetry, and quantum-chemical calculations. The stabilizing effect decreases from $X = F$ to $X = I$. Thermogravimetric

measurements of the salts indicate the loss of the nitric oxide radical (NO^{\bullet}). The homolytic NO^{\bullet} elimination from the dianion under very soft collisional excitation in gas-phase ion experiments results in the formation of the radical $[B_{12}X_{11}O]^{2-\bullet}$. Theoretical investigations suggest that the loss of NO^{\bullet} proceeds via the rearrangement product $[B_{12}X_{11}(ONO)]^{2-}$. The *O*-bonded nitrosooxy structure is thermodynamically more stable than the *N*-bonded nitro structure and its formation by radical recombination of $[B_{12}X_{11}O]^{2-\bullet}$ and NO^{\bullet} is demonstrated.

Introduction

Perhalogenated *closo*-dodecaborate anions $[B_{12}X_{12}]^{2-}$ ($X = F-I$) derive from the parent icosahedral *closo*-dodecaborate anion $[B_{12}H_{12}]^{2-}$ ^[1] and were introduced in 1964 by Muetterties et al.^[2] For the last 15 years they have received increased attention after improved and simple halogenation methods were developed to make these compounds available in large quanti-

ties.^[2,3] Since then, their chemical and physical properties were investigated^[4] and a variety of applications were proposed: perhalogenated *closo*-dodecaborate anions were shown to be weakly coordinating anions capable of stabilizing reactive cations in the condensed phase^[5] and to be suitable counterions for catalytically active cations.^[3d,6] In the solid state, they are part of superacids,^[7] host-guest complexes,^[8] and ion conductors,^[9] while in solution they have interesting properties for electrochemical^[4b] and medicinal applications.^[10] Their gas-phase chemistry is unprecedented^[11] and most recently lead to the discovery of noble-gas-binding molecular anions.^[12]

In recent years, procedures were developed to generate mono-substituted perhalogenated *closo*-dodecaborate anions $[B_{12}X_{11}Y]^{2-}$. In principle, the functional group *Y* enables tuning of the anions' properties for an anticipated application. However, synthetic procedures have only been developed so far for $Y = NR_3^+$, NH_2 , and OR ($R = H$, alkyl).^[13] Introduction of an NR_3^+ group reduces the total charge from -2 to -1 , which leads to better solubility in organic solvents and allowed the synthesis of new ionic liquids.^[13d] While the functional groups $Y = NH_2$, OH and OR reduce the electronic stability of the dianion, a nitro group ($Y = NO_2$) is expected to increase the electronic stability of $[B_{12}X_{11}(NO_2)]^{2-}$ compared to $[B_{12}X_{12}]^{2-}$. The *closo*-borate anions $[B_nH_{n-1}(NO_2)]^{2-}$ ($n = 6, 9, 10$)^[14] and $[B_{12}(OR)_{11}(NO_2)]^{2-}$ ^[15] with one nitro group have been reported, but no halogenated derivatives are known.


Herein, we report the synthesis of $[B_{12}X_{11}(NO_2)]^{2-}$ ($X = F-I$). The perhalogenated *closo*-dodecaborates show exceptional stability against oxidation,^[5,6] which makes them interesting for electrochemical applications. Additionally, an unprecedented reactivity of the boron-bound NO_2 group was investigated,


[a] Prof. Dr. K. R. Asmis, S. Kawa, H. Knorke, Dr. J. Warneke, Z. Warneke
 Wilhelm-Ostwald-Institut für Physikalische und Theoretische Chemie
 Universität Leipzig
 Linnéstr. 2, 04103 Leipzig (Germany)
 E-mail: jonas.warneke@uni-leipzig.de
 Homepage: <https://woi.chemie.uni-leipzig.de/start/nfg-dr-warneke/>

[b] Dr. B. B. Beele, Prof. Dr. C. Jenne, M. C. Nierstenhöfer
 Fakultät für Mathematik und Naturwissenschaften, Anorganische Chemie
 Bergische Universität Wuppertal
 Gaußstr. 20, 42119 Wuppertal (Germany)
 E-mail: carsten.jenne@uni-wuppertal.de
 Homepage: <https://www.molchem.uni-wuppertal.de>

[c] Dr. X.-B. Wang, Dr. Q. Yuan
 Physical Sciences Division
 Pacific Northwest National Laboratory
 902 Battelle Boulevard, Richland, WA 99352 (USA)

[d] Dr. J. Warneke
 Leibniz Institute of Surface Engineering (IOM)
 Permoserstraße 15, 04318 Leipzig (Germany)

 Supporting information and the ORCID identification numbers for the authors of this article can be found under:
<https://doi.org/10.1002/chem.202003537>

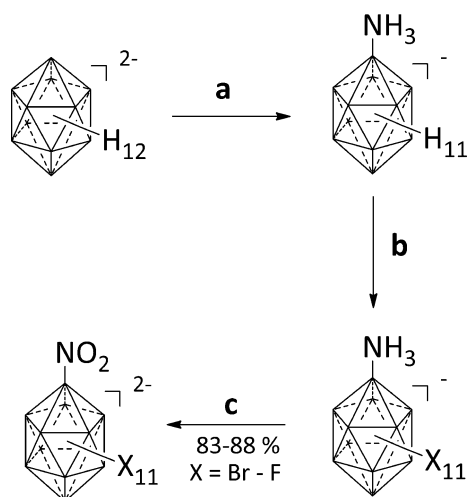
 © 2020 The Authors. Published by Wiley-VCH GmbH. This is an open access article under the terms of the Creative Commons Attribution License, which permits use, distribution and reproduction in any medium, provided the original work is properly cited.

which opens the way to generate highly reactive intermediates from $[B_{12}X_{11}(NO_2)]^{2-}$ ions.

Results and Discussion

Synthesis and characterization of $[B_{12}X_{11}(NO_2)]^{2-}$ ($X = F-I$)

Starting from the parent *closo*-dodecaborate $[B_{12}H_{12}]^{2-}$ the ammonio-substituted perhalogenated clusters $[B_{12}X_{11}(NH_3)]^-$ ($X = F-I$) were obtained in two steps by known procedures.^[13a,e,16] Subsequently, the ammonio group was oxidized with H_2O_2 following a procedure used before for the synthesis of $[B_{12}(OH)_{11}(NO_2)]^{2-}$.^[15,17] For this purpose, the potassium salts of $[B_{12}X_{11}(NH_3)]^-$ were dissolved in an aqueous solution of hydrogen peroxide (30%). Subsequently, potassium hydroxide was added to adjust the pH value to 8–10 (*Caution: A strong gas evolution can occur due to decomposition of H_2O_2 . The use of a burst shield to protect from possible explosion is recommended.*). Aliquots of H_2O_2 were added several times a day and the reaction progress was monitored by ^{11}B NMR spectroscopy. Scheme 1 illustrates the 3-step synthesis starting from $[B_{12}H_{12}]^{2-}$ and full details are given in section S2 of the Supporting Information.



Scheme 1. Reaction sequence to produce $[B_{12}X_{11}(NO_2)]^{2-}$ ($X = F-I$). (a) H_3NOSO_3 , H_2O ^[13a] (b) F_2/N_2 in CH_3CN for $X = F$,^[16] $SbCl_5$ for $X = Cl$,^[13a] Br in H_2O ,^[13e] $I_2 + ICl$, in $C_2H_4Cl_2$ for $X = I$,^[13e,17] (c) $H_2O_2 + KOH$ in H_2O , reflux.^[this work] The given yields correspond to the isolation of the anions as $[N(nBu)_4]^+$ salts. An accurate yield for $X = I$ could not be obtained due to the incomplete conversion. For full synthetic details including precipitation of the anions with different cations see section S2 of the Supporting Information.

The progress of the oxidation of the halogenated *closo*-dodecaborates was monitored over time by NMR spectroscopy. As an example, the ^{11}B and ^{19}F NMR spectra for the reaction of $[B_{12}F_{11}(NH_3)]^-$ with H_2O_2 are shown in Figure 1. The oxidation of the other derivatives was monitored in the same way and a related diagram for $[B_{12}Cl_{11}(NO_2)]^{2-}$ is given in section S2.5 of the Supporting information. At the beginning, the ^{11}B NMR spectrum shows three signals in 1:10:1 ratio. After some time,

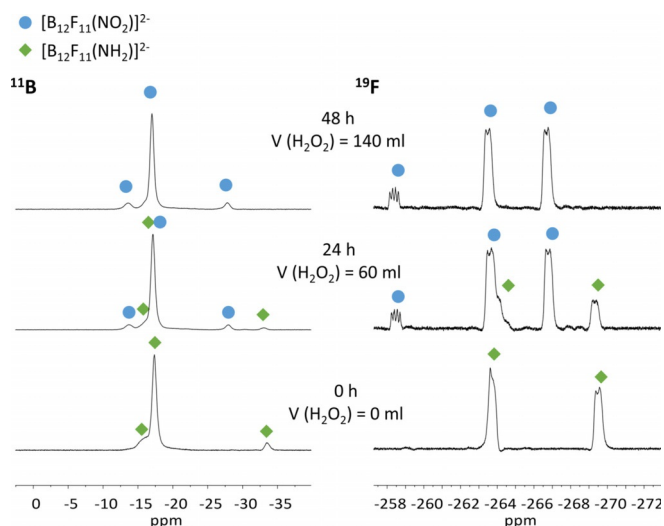
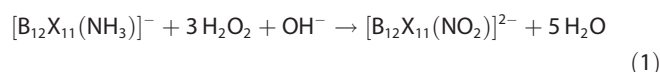


Figure 1. ^{11}B (left) and ^{19}F NMR spectra (right) of the oxidation of $[B_{12}F_{11}(NH_3)]^-$ with H_2O_2 over time. Resonances of the starting material $[B_{12}F_{11}(NH_3)]^-$ are marked with green diamonds and those from the product $[B_{12}F_{11}(NO_2)]^{2-}$ are labeled by blue circles.

a second set of three signals in 1:10:1 ratio appears in the ^{11}B NMR spectrum, which can be assigned to $[B_{12}F_{11}(NO_2)]^{2-}$. ^{11}B - ^{11}B COSY NMR spectra helped to assign the resonances to the respective compounds. In the ^{19}F NMR spectrum the integral ratio of the starting material is 6:5 and splits into a 1:5:5 ratio in the product. Obviously, the chemical shift of the fluorine atom attached to the antipodal boron atom is significantly influenced by the nitro group.

The oxidation of $[B_{12}F_{11}(NH_3)]^-$ requires approximately two days. In the case of $X = Cl$ and $X = Br$ the reaction time increases to approximately ten days and two weeks, respectively. For $[B_{12}I_{11}(NH_3)]^-$ a complete conversion could not be reached even after two weeks. There is a significant increase of reaction time by going from $X = F$ to $X = I$. We calculated reaction energies for the oxidation of $[B_{12}X_{11}(NH_3)]^-$ according to Equation (1), which are highly exergonic (about 700 kJ mol^{-1} for all halogens) and only slightly decreases (by 2%) from $X = F$ to $X = I$ (Table S11 of the Supporting Information). Therefore, different activation energies for the elementary reaction steps are more likely responsible for the observed change in reactivity along the halogen series than the overall reaction enthalpy.



An attack of the nitrogen atom lone electron pair of the amine (the ammonio group is deprotonated under basic conditions) on the H_2O_2 molecule resulting in the formation of an amine oxide may be a simplified representation. The actual mechanism is unknown, but presumably proceeds via different steps involving cyclic transition states.^[18] A large halogen atom X neighbored to the NH_2 group shields the nitrogen atom and certainly causes kinetic barriers due to steric hindrance (see Figure 2). The $B-X$ bond is shorter than the $B-N$ bond for $X = F$, but longer for $X = Cl-I$. In addition, basicity of the NH_2 group

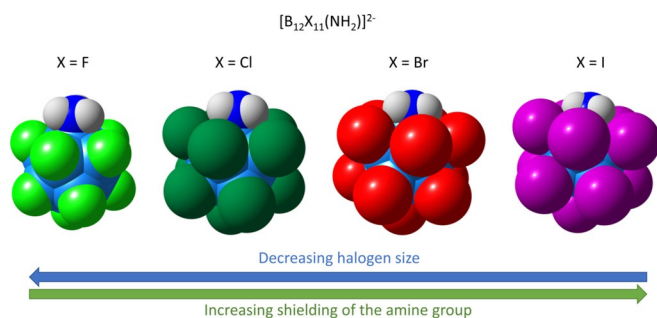


Figure 2. Space-filling models based on PBE0/def2-TZVPP geometries of $[B_{12}X_{11}(NH_2)]^{2-}$ with $X = F-I$. Calculated bond lengths [pm]: $[B_{12}F_{11}(NH_2)]^{2-}$: 149.6 (B–N), 138.3 (B–F); $[B_{12}Cl_{11}(NH_2)]^{2-}$: 147.0 (B–N), 179.7 (B–Cl); $[B_{12}Br_{11}(NH_2)]^{2-}$: 146.3 (B–N), 196.3 (B–Br); $[B_{12}I_{11}(NH_2)]^{2-}$: 145.7 (B–N), 217.1 (B–I).

decreases from $X = F$ to $X = I$ (see Table S10 of the Supporting Information), which may also influence the kinetics of this reaction.

Crystal structures of $[B_{12}X_{11}(NO_2)]^{2-}$ ($X = F-Br$)

A total of nine different crystal structures were measured for $[B_{12}X_{11}(NO_2)]^{2-}$ ($X = F-Br$) with different counter cations such as Cs^+ , $[N(nBu)_4]^+$, $[HNEt_3]^+$, $[PPh_4]^+$, and Ba^{2+} . Most of the obtained crystal structures show positional disorder of the nitro groups. The steric demand of the nitro group is similar to that of the halide substituents and we found examples where the nitro group is disordered over two, four, six, eight or twelve positions, depending on the crystal symmetry and strongly influenced by the counterion and solvent molecules in the lattice. Only for $Cs_2[B_{12}F_{11}(NO_2)] \cdot 2CH_3CN$ and $[N(nBu)_4]_2[B_{12}Br_{11}(NO_2)] \cdot 2CH_3CN$ crystal structures without any positional disorder of the nitro group could be obtained (Figure 3). Visualizations of the anions in the other crystal structures are shown in section S6 of the Supporting Information.

Influence of the nitro group on the electronic properties

In organic chemistry, it is well known that the electron-withdrawing nitro group deactivates aromatics against electrophilic attack while the electron donating amino group leads to activation. The same trend is expected for halogenated *closo*-dodecaborate anions. To evaluate the difference in electronic stability between $[B_{12}X_{11}(NH_2)]^{2-}$, $[B_{12}X_{12}]^{2-}$ and $[B_{12}X_{11}(NO_2)]^{2-}$ ($X = F-I$) we used photoelectron spectroscopy (PES) in the gas phase compared with quantum-chemical calculations and cyclic voltammetry in solution.

The photoelectron spectra measured at a laser wavelength of 157 nm for $X = Cl$ are shown in Figure 4. All other spectra can be found in section S7 of the Supporting Information. In general, the electron donating amino group lowers the electron binding energy of the dianion in the gas phase, while the electron withdrawing nitro group leads to an increase compared to the perhalogenated dianions (Figure 5), in accord with calculated vertical (VDE) and adiabatic detachment ener-

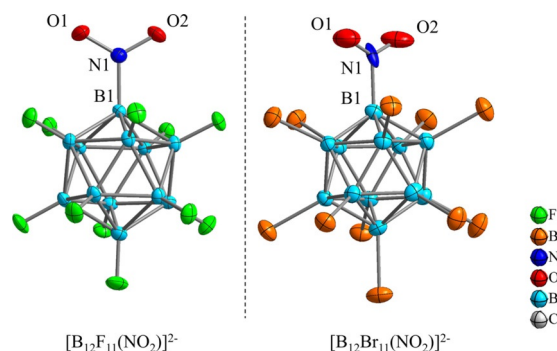


Figure 3. Structure of anions derived from single-crystal X-ray analysis of $Cs_2[B_{12}F_{11}(NO_2)] \cdot 2CH_3CN$ and $[N(nBu)_4]_2[B_{12}Br_{11}(NO_2)] \cdot 2CH_3CN$. Thermal ellipsoids are drawn with 50% probability. Selected experimental and calculated (in *italics*, PBE0/def2-TZVPP) structural parameters (bond lengths in pm and angles in deg.) for $[B_{12}F_{11}(NO_2)]^{2-}$: N1–O1 122.5(2) (122.2), N1–O2 122.3(2) (122.2), B1–N1 154.1(3) (154.9) pm, O1–N1–O2 121.04(19)° (122.4°), B1–N1–O1 119.91(19)° (118.7°), B1–N1–O2 119.05(18)° (118.7°) and $[B_{12}Br_{11}(NO_2)]^{2-}$: N1–O1 111.8(5) (121.7), N1–O2 115.7(5) (121.7), B1–N1 165.3(6) (155.9) pm, O1–N1–O1 129.9(4)° (123.2°), B1–N1–O1 116.0(4)° (118.1°), B1–N1–O2 113.9(4)° (118.1°).

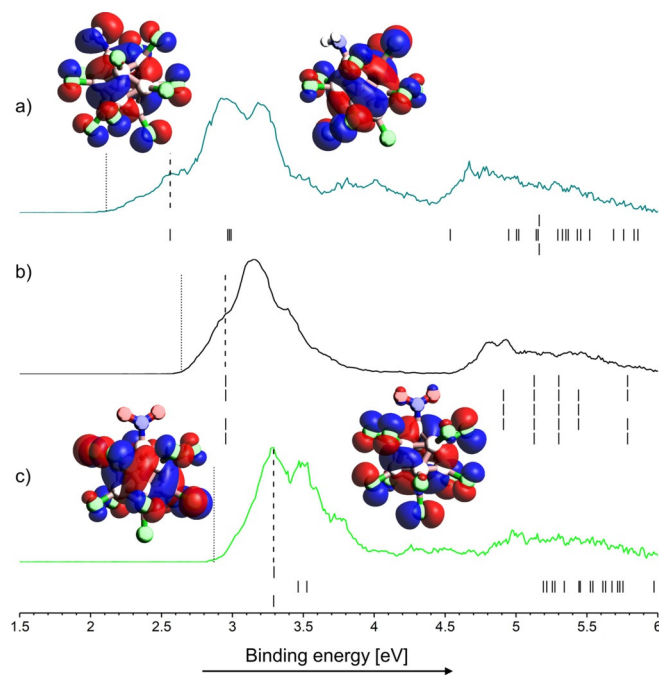


Figure 4. Photoelectron spectra of a) $[B_{12}Cl_{11}(NH_2)]^{2-}$, b) $[B_{12}Cl_{12}]^{2-}$ and c) $[B_{12}Cl_{11}(NO_2)]^{2-}$ measured at 157 nm (7.866 eV). Dashed lines indicate vertical detachment energies (VDE) and dotted lines adiabatic detachment energies (ADE). Density of states (DOS) predicted by Hartree–Fock calculations are shown below the spectra. Note that the energy of all molecular orbitals was shifted by a constant value so that the energy of the highest occupied molecular orbital (HOMO) matches the experimental VDE. The HOMO and HOMO-1 of $[B_{12}Cl_{11}(NH_2)]^{2-}$ and of $[B_{12}Cl_{11}(NO_2)]^{2-}$ are shown. The four highest lying orbitals of all three ions are shown in Figure S43 of the Supporting Information.

gies (ADE) (Table 1). Hartree–Fock-orbital energies (eigenvalues) are plotted below the spectra and shifted in energy so that the energy of the HOMO matches the VDE (Figure 4). The shift compensates for the deviation from Koopman's theorem.

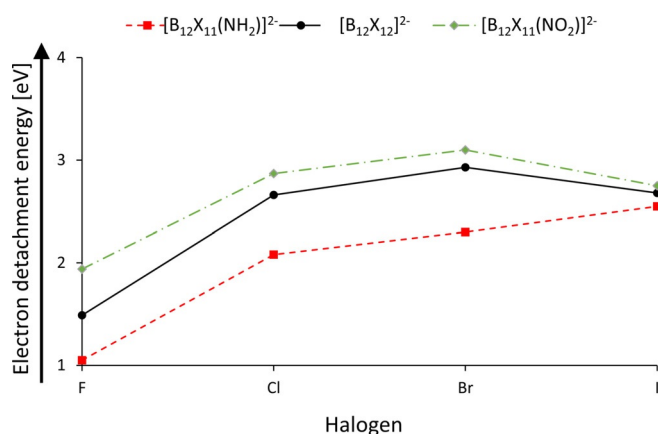


Figure 5. Visualization of the averaged, experimental, adiabatic electron detachment energies of the different substituted *closo*-dodecaborate anions in the gas phase.

For high symmetry $[B_{12}Cl_{12}]^{2-}$ the HOMO is four-fold degenerated. For the lower symmetry $[B_{12}Cl_{11}(NH_2)]^{2-}$ and $[B_{12}Cl_{11}(NO_2)]^{2-}$ ions the energy of the four highest orbitals are differently affected by the functional groups. In the case of $[B_{12}Cl_{11}(NH_2)]^{2-}$, the orbital of the free electron pair of the NH_2 group overlaps with only one of the four highest lying cluster orbitals, significantly destabilizing it energetically. In contrast, the energy of the four highest orbitals are affected by the NO_2 group. While two orbitals are only slightly stabilized and constitute the two-fold degenerate HOMO of $[B_{12}Cl_{11}(NO_2)]^{2-}$, a significant contribution of the oxygen orbitals is present for HOMO-1 and HOMO-2, which are strongly stabilized.

The electronic stabilization caused by the nitro group is strongest for $X=F$ (+0.45 eV). Since $[B_{12}X_{12}]^{2-}$ becomes electronically more stable from $X=F$ to $X=Br$, the additional stabilization affected by substituting one X with NO_2 decreases along the halogen series ($X=Cl$ (+0.21 eV)), $X=Br$ (+0.17 eV). $X=I$ constitutes a special case. While the HOMO for $X=F-Br$ has a significant boron contribution and is influenced by the electronic effect of the substituents Y in $[B_{12}X_{11}Y]^{2-}$, the HOMO

for $X=I$ is almost exclusively localized on the iodine atoms.^[4a] Therefore, the electronic stabilities of $[B_{12}I_{11}NH_2]^{2-}$, $[B_{12}I_{12}]^{2-}$ and $[B_{12}I_{11}NO_2]^{2-}$ are almost identical, see Figure 5.

Complementary to the determination of the electronic stabilities in the gas phase, cyclovoltammetric measurements were performed in liquid sulfur dioxide solution in order to estimate the electrochemical potentials. In the past, liquid sulfur dioxide has been shown to be a suitable solvent for similar *closo*-borate anions with very high oxidation potentials.^[4b,c,19] The cyclic voltammograms for $[B_{12}X_{11}(NO_2)]^{2-}$ ($X=F-Cl$) are shown in section S3 of the Supporting Information. The $[B_{12}X_{11}(NO_2)]^{2-}$ anions for $X=Cl$ and Br show a quasi-reversible redox process, while it is not reversible for $[B_{12}F_{11}(NO_2)]^{2-}$. Compared to $[B_{12}X_{12}]^{2-}$, the oxidation potentials increase in the presence of the nitro group (see Table 1).

These results demonstrate that the electronic properties of $[B_{12}X_{11}Y]^{2-}$ are determined by the choice of Y . NO_2 constitutes a functional group which allows for further chemical modification of the anion.

Reactivity of $[B_{12}X_{11}(NO_2)]^{2-}$ anions

Closo-borate anions are three-dimensional aromatics.^[20] Therefore, it is reasonable to assume that the NO_2 group may be further functionalized by established procedures known for nitrobenzene derivatives. For instance, the reaction with nascent hydrogen obtained by acidifying a heterogenic zinc solution, which is known to reduce aromatic NO_2 groups, generates $[B_{12}X_{11}(NH_3)]^-$ in good yields (section S5 of the Supporting Information). Surprisingly, we observed a thermally induced reaction for $[B_{12}X_{11}(NO_2)]^{2-}$, which is known for nitrobenzene only as a side reaction: In a simultaneous thermogravimetric (TG) and differential scanning calorimetric (DSC) measurement of $[N(nBu)_4]_2[B_{12}X_{11}(NO_2)]$ ($X=F-Br$) in the temperature range from 25 to 350 °C, a step in the TG analysis with onset temperatures between 214 and 248 °C was observed (Figure 6). The detected mass losses are in accord with NO loss from the anion (see Table 2 for experimental and calculated values). The onset tem-

Table 1. Experimental and calculated electron detachment energies in the gas phase and oxidation potentials in SO_2 solution. Energy differences with respect to $[B_{12}X_{12}]^{2-}$ are given in brackets.^[a,b,c]

Anion	Exp. ADE ^[a] [eV] average	Calcd. ADE [eV] ^[b]	Exp. VDE ^[a] [eV] average	Calcd. VDE [eV] ^[b]	E_p^a [c] [V]
$[B_{12}F_{11}(NH_2)]^{2-}$	1.05 (−0.44)	0.72 (−0.58)	1.46 (−0.44)	1.24 (−0.54)	N/A
$[B_{12}F_{12}]^{2-}$	1.49	1.30 ^[4b]	1.90 ± 0.05 ^[4a]	1.78	1.78 ^[6]
$[B_{12}F_{11}(NO_2)]^{2-}$	1.94 (+0.45)	1.69 (+0.39)	2.24 (+0.34)	2.12 (+0.34)	2.09 (+0.31)
$[B_{12}Cl_{11}(NH_2)]^{2-}$	2.08 (−0.58)	1.67 (−0.66)	2.36 (−0.59)	2.05 (−0.58)	N/A
$[B_{12}Cl_{12}]^{2-}$	2.66	2.33 ^[4b]	2.95 ± 0.05 ^[4a]	2.63	2.15 ^[4b]
$[B_{12}Cl_{11}(NO_2)]^{2-}$	2.87 (+0.21)	2.52 (+0.19)	3.18 (+0.23)	2.79 (+0.16)	2.45 (+0.30)
$[B_{12}Br_{11}(NH_2)]^{2-}$	2.30 (−0.63)	1.98 (−0.66)	2.60 (−0.60)	2.33 (−0.56)	N/A
$[B_{12}Br_{12}]^{2-}$	2.93	2.64 ^[4b]	3.20 ± 0.03 ^[4a]	2.89	2.31 ^[4b]
$[B_{12}Br_{11}(NO_2)]^{2-}$	3.10 (+0.17)	2.78 (+0.14)	3.27 (+0.07)	2.99 (+0.10)	2.39 (+0.08)
$[B_{12}I_{11}(NH_2)]^{2-}$	2.55 (−0.13)	2.24 (−0.09)	2.83 (+0.03)	2.27 (−0.07)	N/A
$[B_{12}I_{12}]^{2-}$	2.68	2.33 ^[4b]	2.80 ± 0.02 ^[4a]	2.34	2.1 ^[4b]
$[B_{12}I_{11}(NO_2)]^{2-}$	2.75 (+0.07)	2.39 (+0.06)	2.91 (+0.11)	2.40 (+0.06)	N/A

[a] In order to obtain accurate values measurements at different wavelength were done and averaged (section S7 of the Supporting Information).

[b] PBE0/def2-TZVPP results. [c] The values of cyclovoltammetric measurements were referenced to ferrocene ($E_p^a = 0.06$ in SO_2 ; external standard).

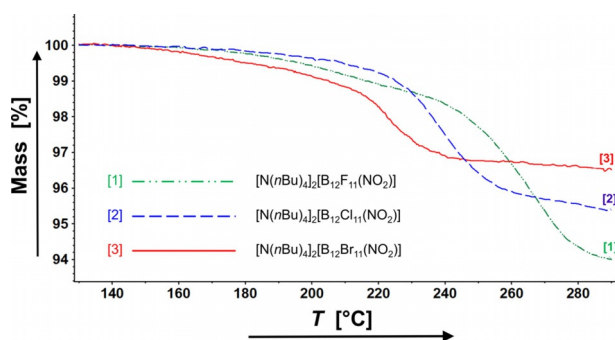


Figure 6. Thermogravimetric analyses of $[N(nBu)_4]_2[B_{12}X_{11}(NO_2)]$ ($X = F, Cl, Br$) with a heating rate of 5 K min^{-1} .

Table 2. Summary of the thermogravimetric and differential scanning calorimetric measurements.				
Compound	T_{onset} [°C]	Mass loss [%]		Exp. reaction enthalpy [kJ mol ⁻¹]
		exp.	calcd.	
$[N(nBu)_4]_2[B_{12}F_{11}(NO_2)]$	248	3.8 ± 0.5	3.5	-79
$[N(nBu)_4]_2[B_{12}Cl_{11}(NO_2)]$	226	3.1 ± 0.5	2.9	-71
$[N(nBu)_4]_2[B_{12}Br_{11}(NO_2)]$	214	1.9 ± 0.5	2.0	-62

peratures in the TG analyses and the reaction enthalpies obtained by the DSC analyses decrease from $[B_{12}F_{11}(NO_2)]^{2-}$ to $[B_{12}Br_{11}(NO_2)]^{2-}$ showing that the stability of the nitro group decreases with increasing halogen size from $X = F - Br$. Decomposition of the organic counterion does not start below 400 °C .

The loss of the radical NO^\bullet as an exclusive reaction at fairly low temperatures from an even electron molecule with an *N*-bonded NO_2 group is surprising. Quantum-chemical calculations suggest that the *N*-bonded NO_2 group is transformed via an η^2-N,O -bonded transition state ($+157\text{ kJ mol}^{-1}$) into an *O*-bonded nitrosooxy moiety ($R-ONO$), which lies several kJ mol^{-1} lower in energy than the *N*-bonded isomer, according to DFT analysis. Subsequently, the ONO -substituted cluster easily eliminates an NO^\bullet molecule (Figure 7).

The change in transition state and reaction enthalpies along the halogen series are qualitatively in agreement with the trend observed in thermogravimetry. A driving force for the rearrangement may be the formation of the strong boron-oxygen bond. For comparison, for nitrobenzene the corresponding transition state is 100 kJ mol^{-1} higher in energy and the nitrosooxy isomer $C_6H_5(ONO)$ is less energetically stable than nitrobenzene^[21] (Figure S41 of the Supporting Information). The remaining $[B_{12}X_{11}O]^{2-}$ radical possesses an oxygen-localized unpaired electron (section S8 and Figure S44 of the Supporting Information) and must be highly reactive. To generate this intermediate, a sample of $Cs_2[B_{12}F_{11}(NO_2)]$ was heated in an open vessel to 300 °C for 40 min and the residue was analyzed by IR, NMR and MS methods and compared to the starting material (spectra are shown in section S4 of the Supporting Information). The ^{11}B NMR spectrum changed from a signal in 1:10:1 ratio to a significantly different pattern in 11:1 ratio (Figure S25 of the Supporting Information), indicating that the B_{12} unit is still present, but has been chemically modified. In the IR

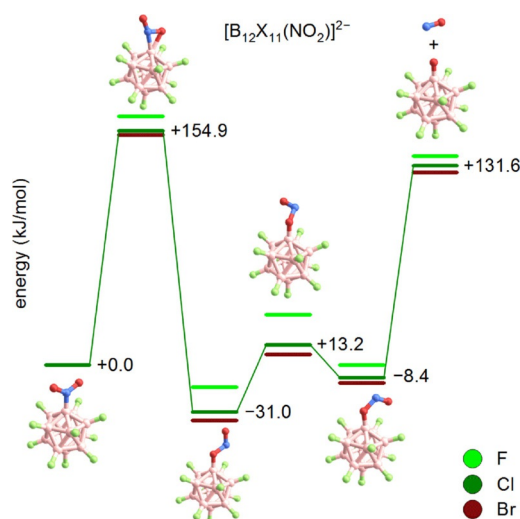


Figure 7. Calculated (B3LYP + GD3BJ/def2-TZVPP) reaction path way for NO^\bullet elimination from $[B_{12}X_{11}(NO_2)]^{2-}$ ($X = F - Br$).

spectrum (Figure S24 of the Supporting Information), the signals assigned to the antisymmetric NO_2 stretch and to the B–N stretch have disappeared and a broad O–H band becomes visible. This is confirmed by the detection of $[B_{12}F_{11}(OH)]^{2-}$ in the mass spectrometric analysis (Figure S26 of the Supporting Information). Since the heated vessel was not protected from ambient molecules like H_2O , $[B_{12}X_{11}(OH)]^{2-}$ is formed by H^\bullet abstraction.

For a direct evidence of the proposed NO^\bullet loss, we aimed for the observation of $[B_{12}X_{11}O]^{2-}$. Due to the ions' high reactivity, potential reaction partners need to be eliminated. Usually, the observation of isolated radical dianions is challenging, because autodetachment of an electron occurs. However, the exceptional electronic stability of halogenated *closo*-borate anions can prevent the dianionic radical from electron emission in the gas phase. Electrospray ionization (ESI) was used to transfer $[B_{12}X_{11}(NO_2)]^{2-}$ into the gas phase of our mass spectrometers. Even at very "soft" conditions (low collisional excitation, see parameters in section S2 of the Supporting Information), ions with m/z 15 smaller than $[B_{12}X_{11}(NO_2)]^{2-}$ were observed. Two experiments were performed to differentiate the ion $[B_{12}X_{11}O]^{2-}$ from the isobar $[B_{12}X_{11}(NH_2)]^{2-}$. (1) High resolution mass spectrometry of $[B_{12}X_{11}O]^{2-}$ distinguishes this ion from $[B_{12}X_{11}(NH_2)]^{2-}$ which was measured for comparison (Figure S55 of the Supporting Information). (2) Structural information on the gaseous ions $[B_{12}Cl_{11}(NO_2)]^{2-}$ and $[B_{12}Cl_{11}O]^{2-}$ were obtained from vibrational spectra using infrared photodissociation spectroscopy (IRPD).^[22] The comparison of the IRPD spectrum of $[B_{12}Cl_{11}(NO_2)]^{2-}$ with harmonic IR spectra (Figure 8a) from DFT calculations shows that the B–N (and not the B–O) bound isomer is present in the gas phase. The symmetric and antisymmetric nitro stretching bands are observed at 1388 cm^{-1} and 1478 cm^{-1} , respectively. In contrast, the IRPD spectrum of $[B_{12}Cl_{11}O]^{2-}$ reveals no IR-active modes of significant intensity above the dominant absorption band at 1032 cm^{-1} (Figure 8b), which is associated with B–Cl stretching

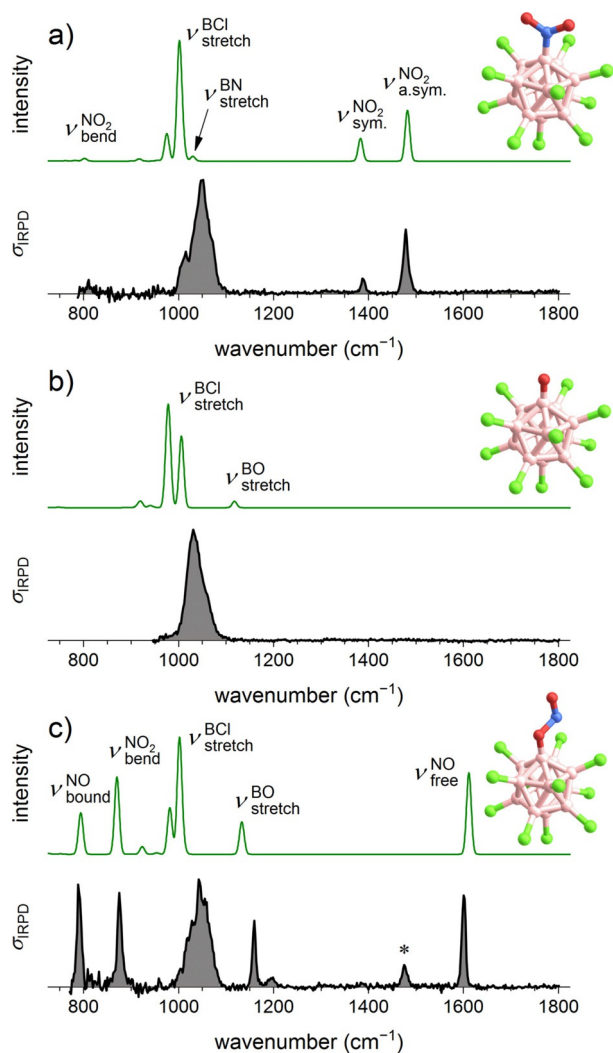


Figure 8. B3LYP + GD3BJ/def2-TZVPP harmonic IR spectra (green) and experimental IRPD spectra of N_2 messenger-tagged ions (black) a) $[B_{12}Cl_{11}(NO_2)]^{2-}$, b) $[B_{12}Cl_{11}O]^{2-}$, and c) $[B_{12}Cl_{11}(ONO)]^{2-}$. The ion $[B_{12}Cl_{11}(ONO)]^{2-}$ was generated by radical recombination of $[B_{12}Cl_{11}O]^{2-}$ and $NO\cdot$. Small amounts of the isobaric $[B_{12}Cl_{11}(NO_2)]^{2-}$ ions due to incomplete fragmentation (for further information see section S2 of the supporting Information) could not be avoided and are responsible for the spectral band marked with an asterisk. See Table S13 of the Supporting Information for band positions and their assignment.

vibrations, coupled to B_{12} -cage deformation modes.^[23] The absence of any NH_2 signals (Figure S46 of the Supporting Information) underlines the assignment and evidences the observation of $[B_{12}Cl_{11}O]^{2-}$. Note, the global minimum-energy structure, the nitrosooxy isomer $[B_{12}Cl_{11}(ONO)]^{2-}$, is not stabilized following collision-induced dissociation (CID) of $[B_{12}Cl_{11}(NO_2)]^{2-}$. The energy necessary to overcome the energy barrier for the NO_2 rearrangement results in bond cleavage and $NO\cdot$ loss. However, the $[B_{12}Cl_{11}(ONO)]^{2-}$ ion, for which so far no synthetic procedure exists, can be generated by gas phase radical recombination of $[B_{12}Cl_{11}O]^{2-}$ with $NO\cdot$. Its IRPD spectrum, shown in Figure 8c, is different from the other two and exhibits a characteristic free $N=O$ stretching band at 1600 cm^{-1} .

The formation and reactivity of $[B_{12}Cl_{11}O]^{2-}$ was further investigated by gas-phase experiments in the presence of coun-

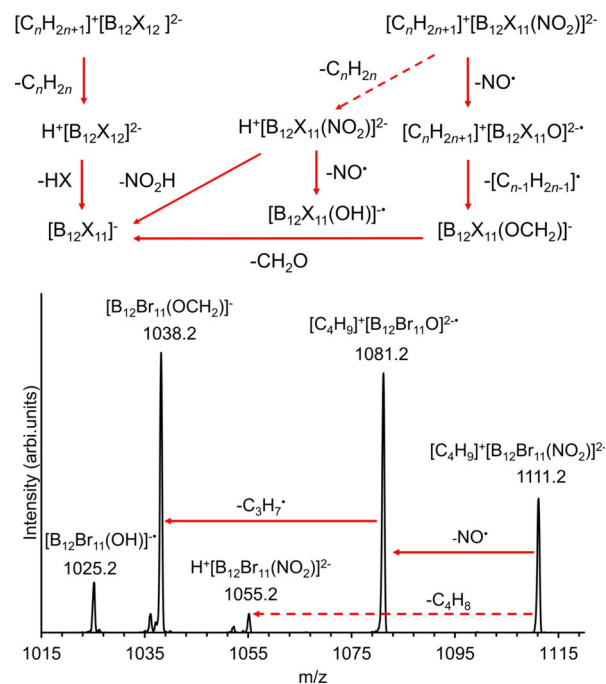


Figure 9. a) Fragmentation scheme of the ion pairs $[C_nH_{2n+1}]^+[B_{12}X_{11}(NO_2)]^{2-}$ and $[C_nH_{2n+1}]^+[B_{12}X_{12}]^{2-}$. While CID of the latter exclusively results in the loss of C_nH_{2n} , this is only a side reaction for $[C_nH_{2n+1}]^+[B_{12}X_{11}(NO_2)]^{2-}$ (indicated by the dashed arrow) and the loss of the $NO\cdot$ is more pronounced. The subsequent loss of $[C_{n-1}H_{2n-1}]^{\cdot}$ transforms the fragment into the even electron ion $[B_{12}X_{11}(OCH_2)]^-$. The fragmentation of both ion pairs finally results in $[B_{12}X_{11}]^-$ (for detailed MS^n analysis confirming the shown pathway for $X=Br$ and for exemplary spectra for $X=Cl$, see section S9 of the Supporting Information). b) CID mass spectrum of the isolated $[C_4H_9]^+[B_{12}Br_{11}(NO_2)]^{2-}$ ion pair showing the $NO\cdot$ and $C_3H_7^{\cdot}$ loss as main fragmentation pathways and the C_4H_8 loss as a side reaction (dashed arrow).

terions. Following an established procedure, alkyl cations $[C_nH_{2n+1}]^+$ ($n=3, 4$) were bound to the dianion by fragmentation of a tetraalkylammonium counterion.^[11a] For the fully perhalogenated clusters, CID of the anionic ion pair $[C_nH_{2n+1}]^+[B_{12}X_{12}]^{2-}$ results in the loss of an alkene and formation of the strong acid $H^+[B_{12}X_{12}]^{2-}$ (see Figure 9a for a fragmentation scheme). In contrast, the equivalent reaction is only observed as a side-reaction for $[C_nH_{2n+1}]^+[B_{12}X_{11}(NO_2)]^{2-}$. The loss of $NO\cdot$ from the ion pair is more pronounced. The resulting radical dianion appears to attack the cation. The next fragmentation step is the loss of the radical $[C_{n-1}H_{2n-1}]^{\cdot}$, which transforms the anion into the even electron system $[B_{12}X_{11}(OCH_2)]^-$ (Figure 9b). The pronounced differences in the fragmentation behavior of $[C_nH_{2n+1}]^+[B_{12}X_{12}]^{2-}$ and $[C_nH_{2n+1}]^+[B_{12}X_{11}(NO_2)]^{2-}$ underline the strong tendency for the loss of $NO\cdot$ and reveal interesting perspectives for reactions with the $[B_{12}X_{11}O]^{2-}$ dianions.

Conclusions

The halogenated $[B_{12}X_{11}(NO_2)]^{2-}$ dodecaborates were obtained in high purity and yield by oxidation of the corresponding amines. This new class of halogenated *closo*-dodecaborates shows improved electrochemical stability compared to the

common $[B_{12}X_{12}]^{2-}$ anions. Their ability to release nitric oxide by thermal treatment gives access to the dianionic oxygen-bound radical $[B_{12}X_{11}O]^{2-}$, which might be a very useful precursor for the chemical modification of the halogenated *closo*-decaborates.

Experimental Section

Numbering scheme, experimental details and spectroscopic data, cyclic voltammetry, thermal NO[•] cleavage, reduction of the nitro group by nascent hydrogen, crystal structures, photoelectron spectroscopy, quantum-chemical calculations, gas phase chemistry are reported in the Supporting Information.

Deposition numbers 2009135, 2009136, 2009137, 2009138, 2009139, 2009140, 2009141, 2009142, and 2009143 contain the supplementary crystallographic data for this paper. These data are provided free of charge by the joint Cambridge Crystallographic Data Centre and Fachinformationszentrum Karlsruhe Access Structures service.

Acknowledgements

M.C.N. is grateful for a Kekulé Fellowship from the Fonds der Chemischen Industrie. J.W. is grateful for a Freigeist Fellowship of the Volkswagen Foundation and thanks Prof. Bernd Abel for providing access to an LTQ Orbitrap-XL. K.R.A. gratefully acknowledges instrumental support from the Fritz-Haber-Institute of the Max-Planck-Society. The photoelectron spectral work was supported by the U.S. Department of Energy (DOE), Office of Science, Office of Basic Energy Sciences, the Division of Chemical Sciences, Geosciences and Biosciences (X.B.W.), and was performed using EMSL, a national scientific user facility sponsored by DOE's Office of Biological and Environmental Research and located at Pacific Northwest National Laboratory, which is operated by Battelle Memorial Institute for the DOE. Open access funding enabled and organized by Projekt DEAL.

Conflict of interest

The authors declare no conflict of interest.

Keywords: boron clusters • electronic stability • gas-phase reactions • mass spectrometry • nitro group • radical ions

- [1] a) I. B. Sivaev, V. I. Bregadze, S. Sjöberg, *Collect. Czech. Chem. Commun.* **2002**, *67*, 679–727; b) A. R. Pitochelli, F. M. Hawthorne, *J. Am. Chem. Soc.* **1960**, *82*, 3228–3229.
- [2] W. H. Knoth, H. C. Miller, J. C. Sauer, J. H. Balthis, Y. T. Chia, E. L. Muetterties, *Inorg. Chem.* **1964**, *3*, 159–167.
- [3] a) I. Tiritiris, T. Schleid, *Z. Anorg. Allg. Chem.* **2004**, *630*, 1555–1563; b) D. V. Peryshkov, A. A. Popov, S. H. Strauss, *J. Am. Chem. Soc.* **2009**, *131*, 18393–18403; c) V. Geis, K. Guttsche, C. Knapp, H. Scherer, R. Uzun, *Dalton Trans.* **2009**, 2687–2694; d) W. Gu, O. V. Ozerov, *Inorg. Chem.* **2011**, *50*, 2726–2728.
- [4] a) J. Warneke, G.-L. Hou, E. Aprà, C. Jenne, Z. Yang, Z. Qin, K. Kowalski, X.-B. Wang, S. S. Xantheas, *J. Am. Chem. Soc.* **2017**, *139*, 14749–14756; b) R. T. Boéré, J. Derendorf, C. Jenne, S. Kacprzak, M. Keßler, R. Riebau, S. Riedel, T. L. Roemmele, M. Rühle, H. Scherer, T. Vent-Schmidt, J. Warneke, S. Weber, *Chem. Eur. J.* **2014**, *20*, 4447–4459; c) R. T. Boéré, S. Kacprzak, M. Keßler, C. Knapp, R. Riebau, S. Riedel, T. L. Roemmele, M. Rühle, H. Scherer, S. Weber, *Angew. Chem. Int. Ed.* **2011**, *50*, 549–552; *Angew. Chem.* **2011**, *123*, 572–575.
- [5] a) I. M. Riddlestone, A. Kraft, J. Schaefer, I. Krossing, *Angew. Chem. Int. Ed.* **2018**, *57*, 13982–14024; *Angew. Chem.* **2018**, *130*, 14178–14221; b) J. Derendorf, C. Jenne, M. Keßler, *Angew. Chem. Int. Ed.* **2017**, *56*, 8281–8284; *Angew. Chem.* **2017**, *129*, 8395–8398; c) C. Bolli, J. Derendorf, M. Kessler, C. Knapp, H. Scherer, C. Schulz, J. Warneke, *Angew. Chem. Int. Ed.* **2010**, *49*, 3536–3538; *Angew. Chem.* **2010**, *122*, 3616–3619; d) J. Derendorf, M. Keßler, C. Knapp, M. Rühle, C. Schulz, *Dalton Trans.* **2010**, *39*, 8671–8678; e) M. Kessler, C. Knapp, V. Sagawe, H. Scherer, R. Uzun, *Inorg. Chem.* **2010**, *49*, 5223–5230; f) M. Kessler, C. Knapp, A. Zogaj, *Organometallics* **2011**, *30*, 3786–3792; g) C. Knapp, C. Schulz, *Chem. Commun.* **2009**, 4991–4993; h) C. Bolli, J. Derendorf, C. Jenne, M. Keßler, *Eur. J. Inorg. Chem.* **2017**, 4552–4558; i) C. Knapp in *Comprehensive Inorganic Chemistry II*, Vol. 1 (Eds.: J. Reedijk, K. Poeppelmeier), Elsevier, Amsterdam, **2013**, pp. 651–679;
- [6] M. Wegener, F. Huber, C. Bolli, C. Jenne, S. F. Kirsch, *Chem. Eur. J.* **2015**, *21*, 1328–1336.
- [7] A. Avelar, F. S. Tham, C. A. Reed, *Angew. Chem. Int. Ed.* **2009**, *48*, 3491–3493; *Angew. Chem.* **2009**, *121*, 3543–3545.
- [8] a) J. Warneke, C. Jenne, J. Bernarding, V. A. Azov, M. Plaumann, *Chem. Commun.* **2016**, *52*, 6300–6303; b) D. V. Peryshkov, A. A. Popov, S. H. Strauss, *J. Am. Chem. Soc.* **2010**, *132*, 13902–13913; c) K. I. Assaf, D. Gabel, W. Zimmermann, W. M. Nau, *Org. Biomol. Chem.* **2016**, *14*, 7702–7706; d) K. I. Assaf, M. S. Ural, F. Pan, T. Georgiev, S. Simova, K. Rissanen, D. Gabel, W. M. Nau, *Angew. Chem. Int. Ed.* **2015**, *54*, 6852–6856; *Angew. Chem.* **2015**, *127*, 6956–6960.
- [9] B. R. S. Hansen, M. Paskevicius, M. Jørgensen, T. R. Jensen, *Chem. Mater.* **2017**, *29*, 3423–3430.
- [10] a) D. Awad, M. Bartok, F. Mostaghimi, I. Schrader, N. Sudumbreakar, T. Schaffran, C. Jenne, J. Eriksson, M. Winterhalter, J. Fritz, K. Edwards, D. Gabel, *ChemPlusChem* **2015**, *80*, 656–664; b) N. S. Hosmane, *Boron science: New technologies and applications*, CRC Press, Boca Raton, **2012**.
- [11] a) J. Warneke, T. Dülcks, C. Knapp, D. Gabel, *Phys. Chem. Chem. Phys.* **2011**, *13*, 5712–5721; b) C. Jenne, M. Keßler, J. Warneke, *Chem. Eur. J.* **2015**, *21*, 5887–5891.
- [12] a) M. Rohdenburg, M. Mayer, M. Grellmann, C. Jenne, T. Borrmann, F. Kleemiss, V. A. Azov, K. R. Asmis, S. Grabowsky, J. Warneke, *Angew. Chem. Int. Ed.* **2017**, *56*, 7980–7985; *Angew. Chem.* **2017**, *129*, 8090–8096; b) M. Mayer, M. Rohdenburg, V. van Lessen, M. C. Nierstenhöfer, E. Aprà, S. Grabowsky, K. R. Asmis, C. Jenne, J. Warneke, *Chem. Commun.* **2020**, *56*, 4591–4594; c) M. Mayer, V. van Lessen, M. Rohdenburg, G.-L. Hou, Z. Yang, R. M. Exner, E. Aprà, V. A. Azov, S. Grabowsky, S. S. Xantheas, K. R. Asmis, X.-B. Wang, C. Jenne, J. Warneke, *Proc. Natl. Acad. Sci. USA* **2019**, *116*, 8167.
- [13] a) C. Bolli, J. Derendorf, C. Jenne, H. Scherer, C. P. Sindlinger, B. Wegener, *Chem. Eur. J.* **2014**, *20*, 13783–13792; b) Y. Zhang, J. Liu, S. Duttwyler, *Eur. J. Inorg. Chem.* **2015**, 5158–5162; c) P. Bertocco, J. Derendorf, C. Jenne, C. Kirsch, *Inorg. Chem.* **2017**, *56*, 3459–3466; d) C. Jenne, C. Kirsch, *Dalton Trans.* **2015**, *44*, 13119–13124; e) J. Holub, S. El Anwar, T. Jelínek, L. Fojt, Z. Růžičková, V. Šolínová, V. Kašička, D. Gabel, B. Grüner, *Eur. J. Inorg. Chem.* **2017**, 4499–4509.
- [14] a) A. Franken, W. Preetz, M. Rath, K. F. Hesse, *Z. Naturforsch. B* **1993**, *48*, 1727–1731; b) K. Siegborg, W. Preetz, *Z. Naturforsch. B* **2000**, *55*, 479–483; c) A. S. Kubasov, E. Y. Matveev, E. S. Turyshv, I. N. Polyakova, K. Y. Zhizhin, N. T. Kuznetsov, *Dokl. Chem.* **2017**, *477*, 257–260.
- [15] A. I. Wixtrom, Z. A. Parvez, M. D. Savage, E. A. Qian, D. Jung, S. I. Khan, A. L. Rheingold, A. M. Spokoiny, *Chem. Commun.* **2018**, *54*, 5867–5870.
- [16] E. V. Bukovsky, A. M. Pluntze, S. H. Strauss, *J. Fluorine Chem.* **2017**, *203*, 90–98.
- [17] O. Bondarev, A. A. Khan, X. Tu, Y. V. Sevryugina, S. S. Jalisatgi, M. F. Hawthorne, *J. Am. Chem. Soc.* **2013**, *135*, 13204–13211.
- [18] R. D. Bach, M.-D. Su, H. B. Schlegel, *J. Am. Chem. Soc.* **1994**, *116*, 5379–5391.
- [19] a) R. T. Boéré, C. Bolli, M. Finze, A. Himmelpach, C. Knapp, T. L. Roemmele, *Chem. Eur. J.* **2013**, *19*, 1784–1795; b) A. Wahab, C. Douvris, J. Klíma, F. Šembera, J. Ugolotti, J. Kaleta, J. Ludvík, J. Michl, *Inorg. Chem.* **2017**, *56*, 269–276.
- [20] a) J. Aihara, *J. Am. Chem. Soc.* **1978**, *100*, 3339–3342; b) J. Poater, M. Solà, C. Viñas, F. Teixidor, *Chem. Eur. J.* **2016**, *22*, 7437–7443; c) J. Aihara,

- Inorg. Chem.* **2001**, *40*, 5042–5044; d) R. B. King, *Chem. Rev.* **2001**, *101*, 1119–1152; e) M. Zhao, B. M. Gimarc, *Inorg. Chem.* **1993**, *32*, 4700–4707.
- [21] a) Y. Peng, X. Xiu, G. Zhu, Y. Yang, *J. Phys. Chem. A* **2018**, *122*, 8336–8343; b) R. Yang, X. Jin, W. Wang, K. Fan, M. Zhou, *J. Phys. Chem. A* **2005**, *109*, 4261–4266; c) M. L. Hause, N. Herath, R. Zhu, M. C. Lin, A. G. Suits, *Nat. Chem.* **2011**, *3*, 932–937; d) T. H. Osterheld, T. Baer, J. I. Brauman, *J. Am. Chem. Soc.* **1993**, *115*, 6284–6289.
- [22] H. Schwarz, K. R. Asmis, *Chem. Eur. J.* **2019**, *25*, 2112–2126.
- [23] L. A. Leites, S. S. Bukalov, A. P. Kurbakova, M. M. Kaganski, Y. L. Gaft, N. T. Kuznetsov, I. A. Zakharova, *Spectrochim. Acta Part A* **1982**, *38*, 1047–1056.

Manuscript received: July 29, 2020

Revised manuscript received: August 10, 2020

Version of record online: October 5, 2020